

Discovery of an X-ray nebula around PSR J1718–3825 and implications for the nature of the γ -ray source HESS J1718–385

J.A. Hinton¹, S. Funk², S. Carrigan³, Y.A. Gallant⁴, O.C. de Jager⁵, K. Kosack³, A. Lemi re⁶, and G. P hlhofer⁷

¹ School of Physics & Astronomy, University of Leeds, Leeds LS2 9JT, UK

² Kavli Institute for Particle Astrophysics and Cosmology, SLAC, 2575 Sand Hill Road, Menlo-Park, CA-94025, USA

³ Max-Planck-Institut f r Kernphysik, P.O. Box 103980, D 69029 Heidelberg, Germany

⁴ Laboratoire de Physique Th orique et Astroparticules, CNRS/IN2P3, Universit  Montpellier II, CC 70, Place Eug ne Bataillon, F-34095 Montpellier Cedex 5, France

⁵ Unit for Space Physics, North-West University, Potchefstroom 2520, South Africa

⁶ CFA - Harvard, 60 Garden Street, 02138 Cambridge MA, USA

⁷ Landessternwarte, Universit t Heidelberg, K nigstuhl, D 69117 Heidelberg, Germany

Received; Accepted

ABSTRACT

Combined X-ray synchrotron and inverse-Compton γ -ray observations of pulsar wind nebulae (PWN) may help to elucidate the processes of acceleration and energy loss in these systems. In particular, such observations provide constraints on the particle injection history and the magnetic field strength in these objects. The newly discovered TeV γ -ray source HESS J1718–385 has been proposed as the likely PWN of the high spin-down luminosity pulsar PSR J1718–3825. The absence of previous sensitive X-ray measurements of this pulsar, and the unusual energy spectrum of the TeV source, motivated observations of this region with *XMM-Newton*. The data obtained reveal a hard spectrum X-ray source at the position of PSR 1718–3825 and evidence for diffuse emission in the vicinity of the pulsar. We derive limits on the keV emission from the centroid of HESS J1718–385 and discuss the implications of these findings for the PWN nature of this object.

Key words. pulsars:PSR J1718–3825, X-rays:observations, gamma-rays:observations

1. Introduction

Young pulsars drive relativistic winds into their environments, confinement of which leads to the production of extremely broadband emission via the synchrotron and inverse-Compton (IC) processes (see Gaensler & Slane 2006, for a recent review). The most prominent PWN, the Crab Nebula, is detected in all wavebands from the radio to TeV γ -rays (Weekes et al. 1989), with the transition from synchrotron to IC emission at ~ 1 GeV. The recent increase in sensitivity of ground-based TeV γ -ray instruments has led to a rapid increase in the number of putative PWN in this waveband. These objects are characterised by diffuse, typically offset, nebulae around high spin-down luminosity pulsars. The archetype of this new object class is the PWN G 18.0–0.7/HESS J1825–137. G 18.0–0.7 is a $\sim 5'$ long asymmetric X-ray synchrotron nebula associated with the middle-aged (characteristic spin-down age $\tau=21$ kyr) pulsar PSR B1823–13 (Gaensler et al. 2003). The IC nebula HESS J1825–137 is much larger ($\sim 100'$ at 1 TeV) but exhibits energy-dependent morphology, shrinking towards the pulsar at high energies (Aharonian et al. 2006b; Funk et al. 2007a), suggestive of cooling of the highest-energy (X-ray synchrotron emitting) electrons away from the pulsar.

The TeV γ -ray source HESS J1718–385 was discovered in deep observations of the supernova remnant RX J1713.7–3946 using H.E.S.S. in 2004–2005 (Aharonian et al. 2007). The absence of other potential counterparts and the relatively compact nature of the source ($9' \times 4'$ rms) make an association with PSR J1718–3825 ($8'$ from the centroid of the TeV source) plausible. The TeV source is unusual in its sharply peaked spectral

energy distribution (SED), which is similar to that of the γ -ray nebula of the Vela pulsar (Aharonian et al. 2006a). The γ -ray emission from these objects is commonly attributed to IC scattering of relativistic electrons (see Horns et al. 2006, for an alternative view). In this scenario the spectral break seen at ~ 10 TeV in these objects can be interpreted as a signature of electron cooling. However, PSR J1718–3825 (estimated distance 4.2 pc) has a characteristic spin-down age (90 kyr) almost an order of magnitude greater than that of the Vela pulsar, making such a high energy break very surprising.

The search for a possible X-ray counterpart to HESS J1718–385 is important for two reasons: firstly, to verify the identification of the TeV source as the PWN of PSR J1718–3825 and secondly, to explore the physical conditions and electron energy distribution in the putative nebula. As no sensitive X-ray observations of the PSR J1718–3825/HESS J1718–385 region existed, *XMM-Newton* was used to observe this region in September 2006.

2. Observations and Analysis

Observations of HESS J1718–385 with *XMM-Newton* were conducted on the 4th of September 2006 (Obs.-ID 0401960101). Data of 22.3 ks duration were obtained with all X-ray instruments (PN, MOS1, MOS2) operating in the full-frame mode with a medium filter. Our analysis utilises the *XMM-Newton* Science Analysis Software (SAS), version 7.0, together with the Extended Source Analysis Software package (*XMM-ESAS*), version 1.0 (Snowden et al. 2004). The diffuse-source analy-

sis required the development of our own software extensions. Following standard calibration and data reduction, the data were cleaned of soft proton flares, reducing the usable observation time to 15.2 ks.

ID	XMMUJ	RA 17h	Dec. −38°	Counts
1	171813.8–382517	18 ^m 13.79 ^s	25′16.6″	256
2	171808.8–382604	18 ^m 08.80 ^s	26′04.0″	255
3	171833.0–382749	18 ^m 33.04 ^s	27′48.9″	154
4	171830.9–382704	18 ^m 30.94 ^s	27′03.7″	152
5	171824.5–383204	18 ^m 24.49 ^s	32′04.2″	114
6	171805.1–383140	18 ^m 05.09 ^s	31′40.5″	100
7	171723.8–383233	17 ^m 23.75 ^s	32′32.8″	95
8	171803.5–383315	18 ^m 03.54 ^s	33′14.6″	79
9	171853.7–382228	18 ^m 53.74 ^s	22′28.0″	73
10	171847.8–384158	18 ^m 47.79 ^s	41′58.2″	63

Table 1. Properties of the 0.5–10 keV X-ray point sources found in the *XMM-Newton* observation described here, ranked by the number of excess counts detected. The statistical errors on the source positions lie in the range 0.5–1.4″.

Following the standard *XMM-Newton* point-source identification procedure, ten sources are detected in the combined MOS1+MOS2 data (see table 1). Each of these sources is detected in all three standard energy bands (0.5–2 keV, 2–4.5 keV, 4.5–10 keV). The brightest source in the field of view (source #1) is coincident with PSR J1718–3825. The other bright sources in the field appear to be associated with stars: sources #2,#3 and #4 with HD 323016, HD 323015 and HD 323014, respectively. A smoothed and vignetting-corrected 0.5–10 keV image is presented in the left panel of Figure 1, with the source fit positions marked. Neither of the two previously known X-ray sources in the field of view (both ROSAT All-sky survey faint sources) were detected, suggesting that these may be simply statistical fluctuations (both are $\sim 3\sigma$ detections) or are perhaps variable sources. The best-fit position of source #1 lies 2″ away from the pulsar position. The pointing accuracy of the dataset is estimated at $\sim 2″$ from the offsets of sources #2, #3 and #4 from their stellar counterparts, consistent with the specifications of the MOS detectors. We therefore conclude that source #1 is positionally coincident with PSR J1718–3825 and also falls within the region of TeV emission HESS J1718–385. The source position fitting tool *emldetect* also tries to determine an extension for each source using a Gaussian emission model. None of the sources is found to be significantly extended with this tool, however, an additional spurious source is consistently found to the east of source #1 which is not visible upon inspection, suggesting a possible extension of source #1.

A point-source spectral analysis of source #1 using all available data (MOS1, MOS2 and PN) within a radius of 19″ yields acceptable goodness-of-fit for an absorbed power-law spectrum with photon index $\Gamma = 1.47 \pm 0.21$, a normalisation of $N_0 = 2.4_{-0.5}^{+0.9} \times 10^{-5} \text{ cm}^{-2} \text{ s}^{-1} \text{ keV}^{-1}$ and an absorbing column $n_{\text{H}} = 2.9_{-1.0}^{+1.4} \times 10^{21} \text{ cm}^{-2}$ resulting in a flux of $F_{2-10 \text{ keV}} \approx 1.4 \times 10^{-13} \text{ erg cm}^{-2} \text{ s}^{-1}$. The best fit n_{H} seems somewhat low considering the column density of $\approx 2.8 \times 10^{21} \text{ cm}^{-2}$ in the molecular component alone (estimated by integrating the ^{12}CO data of Dame et al. (2001) out to 4.2 kpc). For a typical molecular to atomic ratio (in the range 2–5) one might expect a value close to $8 \times 10^{21} \text{ cm}^{-2}$. This picture is also consistent with mean HI column density

through the entire galaxy for the field of view (FoV) is a whole: $1.2 \times 10^{22} \text{ cm}^{-2}$. A fit with an absorbed black-body spectrum does not converge due to the small number of counts, fitting with a non-absorbed thermal spectrum yields $kT = 1.00 \pm 0.06 \text{ keV}$, and a flux of $F_{2-10 \text{ keV}} \approx 1.1 \times 10^{-13} \text{ erg cm}^{-2} \text{ s}^{-1}$. Fixing n_{H} at $8 \times 10^{21} \text{ cm}^{-2}$ reduces the best-fit temperature to $kT = 0.74 \pm 0.02 \text{ keV}$. Thermal emission from the neutron star surface seems very unlikely given the high temperature (see for example Page 1997) and the emission can be interpreted as non-thermal emission from the pulsar and an unresolved PWN component. Fixing n_{H} to the same value for a power-law fit yields $\Gamma = 1.95 \pm 0.08$. For all the spectral fitting, the background was taken from a ring surrounding the source #1 (avoiding source #2) with inner radius 95″ and outer radius 180″. Given the frame integration times of both the MOS (2 s) and PN (73 ms) cameras in full frame mode, it was not possible to search for pulsed emission from source #1 at the period of PSR J1718–3825 (74.7 ms).

To search for diffuse emission, a mask was produced to remove sources and regions of less than 30% of the peak exposure in the combined MOS1+MOS2 data. This mask is applied to both the count map (after subtraction of the estimated particle background) and the exposure map, which are then smoothed and the ratio taken to yield a vignetting-corrected source-subtracted map (see the right panel of Figure 1). There is evidence for diffuse emission peaking close to PSR J1718–3825 with a general gradient in the North-South direction. To test the hypothesis that the non-uniformity of the large-scale diffuse emission is due to foreground absorption, we compare the diffuse map to a $8 \mu\text{m}$ GLIMPSE image of the region—intended to trace dust and hence molecular material along the line-of-sight. An anti-correlation seems to be present, with the possibility of substantial absorption towards the centroid of the H.E.S.S. source. However, such absorption does not seem to be supported by the energy dependence of the diffuse emission morphology—which remains roughly constant with energy. Note that the features at the FoV edge may be due to under-subtraction of the particle background (Snowden et al. 2004). To determine the energy distribution of the diffuse component around source #1, a spectrum within an annulus of outer radius 60″ and inner radius 19″ has been determined. A fit of an absorbed power-law spectrum yields a photon index of $\Gamma = 1.86_{-0.13}^{+0.22}$, an absorbing column n_{H} of $7.2_{-0.8}^{+3.0} \times 10^{21} \text{ cm}^{-2}$ and a flux of $F_{2-10 \text{ keV}} \approx 1.3 \times 10^{-13} \text{ erg cm}^{-2} \text{ s}^{-1}$ —very similar to the total flux from the central point source #1. Fixing $n_{\text{H}} = 8 \times 10^{21} \text{ cm}^{-2}$ results in $\Gamma = 1.84 \pm 0.09$. There is therefore no evidence for a spectral softening away from the pulsar, as seen for example in G 18.0–0.7, at least not for the inner 1′. A fit for the full 1′ radius region yields $\Gamma = 1.69_{-0.09}^{+0.15}$.

Interpretation of the SED requires measurements with matching spatial extent. In the absence of a morphological match between the TeV and diffuse keV emission we can only derive upper limits on the direct X-ray counterpart to the extended nebula of HESS J1718–385. To this end, East-West slices (with a North-South extent matched to the rms extent of the H.E.S.S. source) were made through the vignetting-corrected, and source-subtracted MOS1+MOS2 count map. These slices are then fit to a model of a flat background plus a Gaussian component with an rms width constrained to be within a factor 2 of that of the H.E.S.S. source. The 95% confidence upper limits on the number of counts in this Gaussian component are converted into flux upper limits in two energy bands (see Figure 2) under the assumption of a $\Gamma = 2$ spectrum and an absorbing column of $1.2 \times 10^{22} \text{ cm}^{-2}$. As the absorbing column may be significantly higher than this over part of this region it is important to assess

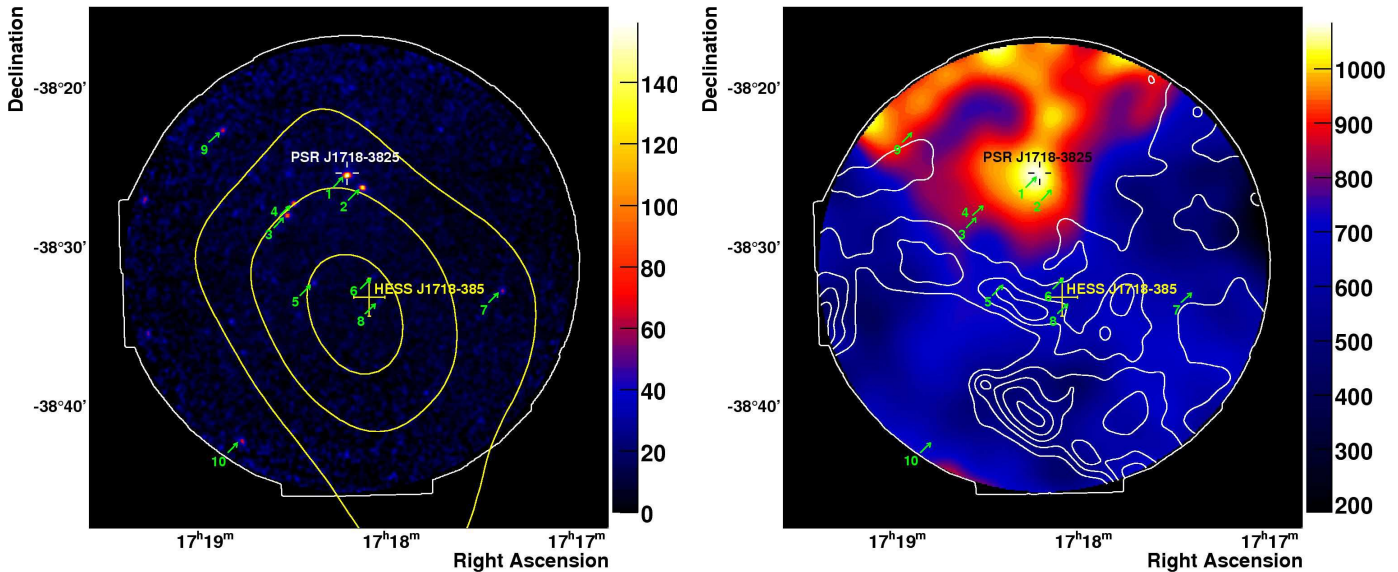


Fig. 1. *Left:* XMM-Newton 0.5–10 keV combined MOS1 and MOS2 image of the vicinity of HESS 1718–385 (colour-scale) compared to the TeV γ -ray morphology (contours). The X-ray data are vignetting-corrected and smoothed with a Gaussian of rms $6''$. The sources summarised in table 1 are identified by arrows. The edge of the FoV of the combined MOS1, MOS2 images is indicated as a white line. The statistical error on the position of the centroid of HESS J1718–385 is indicated by a cross. The radio position of PSR J1718–3825 is also marked. *Right:* Image of diffuse 0.5–10 keV X-ray emission in the same FoV of (colour scale). The XMM-Newton combined MOS1+MOS2 data have been point-source-subtracted and smoothed with a Gaussian of $\sigma = 1'$ (see text for details). The positions of the subtracted sources are marked with arrows. The contours show *Spitzer* $8\mu\text{m}$ data from the GLIMPSE survey, smoothed with $\sigma = 30''$.

the impact of additional absorption on these limits. A factor two increase in the n_H assumed increases the 0.5–2 keV limit by a factor 3, but the 2–4.5 keV limit by only 30%.

3. Discussion

The discovery of hard spectrum X-ray emission from the vicinity of PSR J1718–3825, and the evidence for a diffuse halo around the pulsar strongly suggest the existence of a synchrotron nebula around this pulsar. This discovery strengthens the association of the γ -ray source HESS J1718–385 to PSR J1718–3825, but the relationship of the X-ray emission to the γ -ray source is not straightforward. The overall asymmetry of the nebula with respect to the pulsar is consistent with the idea of SNR expansion into a non-uniform molecular environment (see for example Blondin et al. 2001). The very different morphologies in the two wavebands suggest that either electrons of rather different energies are responsible for the two sources and/or that the magnetic field strength within the nebula is highly non-uniform. As the target for IC emission is the CMBR and other large-scale radiation fields, the IC flux F_{IC} is simply proportional to the number of radiating electrons, n_e , whereas the synchrotron flux goes as: $F_{\text{synch}} \propto B^2 n_e$. In either case the situation may be rather similar to that of HESS J1825–137 or indeed HESS J1813–178 (Funk et al. 2007b), with the lifetime of TeV γ -ray emitting electrons being longer than the age of the pulsar, and having time to propagate over distances of several parsecs. The SED of the source is presented in Figure 2. Three features are of note:

1) a hard IC spectrum at TeV energies, with a peak at ~ 10 TeV. This suggests that the electrons responsible for this emission are uncooled. This is rather surprising given the spin-down age of the pulsar (90 kyr): cooling on the CMBR alone

would result in a spectral break at 2 TeV after 90 kyr, inconsistent with the γ -ray data. Indeed ages > 40 kyr appear to be excluded by the data. A true age of ~ 10 kyr could be explained by a birth period for the pulsar very close to its current period of 75 ms, or breaking deviating significantly from the pure magnetic dipole case (as it seems may commonly be the case, see Kramer et al. (2006))¹. The shape of the TeV spectrum appears to be consistent with a constant injection of (mono-energetic) ~ 70 TeV electrons (curve **A**), or with a hard power-law (index ≈ 1.8) with a sharp cut-off around 100 TeV (**C**).

2) hard spectrum X-ray emission from the pulsar vicinity with a much lower energy flux. The spectrum from within $1'$ of PSR J1718–3825 shown in Figure 2 represents the combined flux of pulsar itself and the inner PWN. The pulsar contribution is certainly less than half of the total emission (as is clear from the flux in the annulus surrounding the pulsar) and for typical systems of this type represents only $\sim 20\%$ of the PWN emission in the $> 2\text{keV}$ range (Kargaltsev et al. 2007). Assuming the PWN is dominant, the hard spectrum suggests either higher electron energies or larger magnetic fields in this region (**B**) in comparison to those found in the γ -ray nebula. The lower flux can be explained if only recently injected electrons are confined in the region around the pulsar. Whilst the two-zone scenario illustrated by curves **A** and **B** is clearly grossly oversimplified, it does appear that the data are consistent with the idea that electrons with a relatively narrow energy distribution rapidly escape from a high B -field region close to the pulsar into the extended

¹ We further note that the projected length of the γ -ray nebula (~ 10 pc) is roughly half that of HESS J1825–137, despite the fact that PSR J1718–3825 is apparently a factor 5 older. Another possibility is that HESS J1825–137 represents only the youngest part of a larger, softer spectrum, γ -ray nebula.

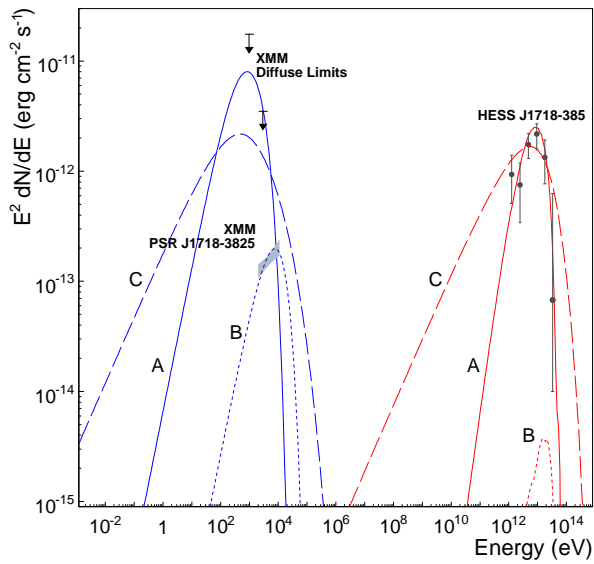


Fig. 2. Spectral energy distribution for the pulsar wind nebula of PSR J1718–3825. The de-absorbed spectrum of emission from within $1'$ of the pulsar is shown together with limits for diffuse emission from the region covered by HESS J1718–385. Three sets of illustrative synchrotron and inverse Compton model curves are shown, based on assumptions of: **A**) Mono-energetic 70 TeV electrons injected over a 10^4 year period, $B = 5\mu\text{G}$, **B**) 70 TeV electrons, $B = 20\mu\text{G}$, $t = 8$ years and **C**) An electron energy distribution following a power-law ($\alpha = 1.8$) with an abrupt cut-off at 100 TeV. These curves are calculated as described in Hinton & Aharonian (2007).

nebula seen in γ -rays. Another plausible scenario is that the injection spectrum of electrons has changed significantly over the lifetime of the pulsar.

3) the energy flux level of diffuse X-ray emission from the HESS J1718–385 region exceeds the TeV flux by not more than a factor ~ 2 . The energy distribution of electrons is essentially fixed by the TeV data. The diffuse X-ray limits can therefore be used constrain the B -field in the extended nebula to be not much greater than $5\mu\text{G}$ (curves **C+A**), close to the mean value of the ISM. We note that this constraint comes principally from the diffuse limit at 2–4.5 keV which is relatively independent of the assumed absorbing column.

In conclusion, the diffuse X-ray emission around XMMU 171813.8–382517 and HESS J1718–385 appear to represent different zones in the PWN of the middle-aged pulsar PSR J1718–3825. Future studies of this complex system are certainly well motivated. For example, with the superior angular resolution of Chandra, the contribution of the pulsar itself to the non-thermal emission could be separated from that of the PWN.

References

- Aharonian, F., Akhperjanian, A. G., Bazer-Bachi, A. R., et al. 2007, A&A, 472, 489
 Aharonian, F., Akhperjanian, A. G., Bazer-Bachi, A. R., et al. 2006a, A&A, 448, L43
 Aharonian, F., Akhperjanian, A. G., Bazer-Bachi, A. R., et al. 2006b, A&A, 460, 365
 Blondin, J. M., Chevalier, R. A., & Frierson, D. M. 2001, ApJ, 563, 806
 Dame, T. M., Hartmann, D., & Thaddeus, P. 2001, ApJ, 547, 792
 Funk, S., Hinton, J. A., & de Jager, O. C. 2007a, ArXiv e-prints, 709.3125

- Funk, S., Hinton, J. A., Moriguchi, Y., et al. 2007b, A&A, 470, 249
 Gaensler, B. M., Schulz, N. S., Kaspi, V. M., Pivovarov, M. J., & Becker, W. E. 2003, ApJ, 588, 441
 Gaensler, B. M. & Slane, P. O. 2006, ARA&A, 44, 17
 Hinton, J. A. & Aharonian, F. A. 2007, ApJ, 657, 302
 Horns, D., Aharonian, F., Santangelo, A., Hoffmann, A. I. D., & Masterson, C. 2006, A&A, 451, L51
 Kargaltsev, O., Pavlov, G. G., & Garmire, G. P. 2007, ApJ, 660, 1413
 Kramer, M., Lyne, A. G., O'Brien, J. T., Jordan, C. A., & Lorimer, D. R. 2006, Science, 312, 549
 Page, D. 1997, ApJ, 479, L43
 Snowden, S. L., Collier, M. R., & Kuntz, K. D. 2004, ApJ, 610, 1182
 Weekes, T. C., Cawley, M. F., Fegan, D. J., et al. 1989, ApJ, 342, 379